Chemical Science

ROYAL SOCIETY OF CHEMISTRY

EDGE ARTICLE

View Article Online
View Journal | View Issue

Cite this: *Chem. Sci.*, 2023, **14**, 4620

All publication charges for this article have been paid for by the Royal Society of Chemistry

Received 7th December 2022
Accepted 7th March 2023

DOI: 10.1039/d2sc06738b

rsc.li/chemical-science

Single-atom copper catalyst for the *S*-arylation reaction to produce diaryl disulfides†

Yiming Zhao, Yan Zhou, Shanshan Lv, Han Li, Qikang Wu, Shaohuan Liu, Wanying Li, Taiyu Chen and Zheng Chen *

Single-atom Cu supported on CeO_x nanorod catalysts (Cu_1/CeO_x) have been synthesized through the anchoring of copper by terminal hydroxyl groups on the CeO_x surface. The oxygen defect characteristics of the CeO_x nanorods promote electron transfer between Cu and CeO_x through a Ce–O–Cu interface, which realizes flexible electronic regulation of the Cu sites. Single-atom Cu species with an oxidation state of between +1 and +2 were formed, which was confirmed by X-ray photoelectron spectroscopy, X-ray fine structure spectroscopy, and electron paramagnetic resonance spectroscopy. Cu_1/CeO_x emerged as a catalyst with advanced catalytic performance for elemental sulfur in *S*-arylation using aryl iodides, achieving 97.1% iodobenzene conversion and 94.8% selectivity toward diphenyl disulfide. The substituted iodobenzene with different electronic or steric groups successfully realized *S*-arylation and produced the corresponding diaryl disulfides with high selectivity. The fully exposed single-atom Cu with flexible electronic characteristics successively realized oxidative addition or coordination of multiple substrates, making it possible to obtain diaryl disulfide with high selectivity.

Introduction

Transition-metal oxides (TMOs) have been widely used as supports for the preparation of single-atom metal catalysts, which show unique catalytic properties in heterogeneous catalysis.[1–4] Single metal atoms are usually anchored in the oxygen vacancies[5–8] or metal vacancies[9–12] generated by TMOs, or other coordination unsaturated sites, such as edges, steps and terraces.[13–16] Through metal–support interactions (MSI), not only can a single metal atom is stabilized, but also the electronic structure of the metal can be adjusted, especially on reducible TMOs.[17–21] Although the metal utilization of single-atom catalysts can be maximized compared with nanoparticles, the steric hindrance of the metal center in the above anchoring types is large because metal atoms are embedded in the lattice structure. This not only has a great impact on the simple reaction of small molecule activation, it also hinders the reaction of multiple complex substrates on a single metal site. Cerium oxide (CeO_x) easily produces oxygen vacancies due to the coexistence of +3 and +4 valence states, which are used as support to anchor single metal atoms in automobile exhaust elimination and industrial catalytic processes.[22,23] The anchoring effect of hydroxyl groups on a CeO_x surface to metal species during the preparation of catalysts is usually ignored and rarely considered as sites for anchoring single atoms, although many examples of CeO_x-anchored single-atom Cu have been reported. Although the surface hydroxyl groups of CeO_x will be removed after heat treatment, it is inevitable that it will come into contact with oxygen and water in the atmospheric environment or in aqueous solutions of metal salts. In this way, the hydroxyl groups on the surface of CeO_x will still exist and play an important role in the anchoring of metal species.[1,24] MSI still exist in this type of single-atom metal catalyst after heat treatment and electron transfer can be realized through a metal-O-Ce interface.[25,26] Compared with vacancy-anchored single-atom metal species, the anchoring of surface hydroxyl groups is conducive to the full exposure of single metal atoms, which is more favorable for application in the transformation of complex organic molecules, especially the activation of multiple substrates.

Diaryl disulfide compounds are valuable reagents in organic synthesis due to their unique S–S bonds, which exhibit high activity in radical tandem reactions or transition metal catalyzed pathways to synthesis functional sulfur-containing organic compounds.[27–29] With the special properties of organic disulfides and the continuous development of their application in synthetic chemistry and biochemistry,[30,31] the synthesis of disulfides has also been greatly developed. Using elemental sulfur as a sulfur source is an advanced alternative to constructing C–S bonds in the synthesis of functional materials and biological compounds, which has the advantages of being odorless, tasteless, stable, and cheap, and having no need for pre-functionalization.[32,33] Through the transition metal

Key Laboratory of Functional, Ministry of Education, College of Chemistry and Materials Science, Anhui Normal University, Wuhu 241000, China. E-mail: chenzh07@mail.ahnu.edu.cn

† Electronic supplementary information (ESI) available. See DOI: https://doi.org/10.1039/d2sc06738b

catalyzed *S*-arylation reaction, the coupling of aryl halides and elemental sulfur can result in the formation of aryl disulfides or aryl sulfides.[34,35] However, the preferentially formed disulfide products continue to react with the substrate aryl iodides to form diarylsulfides or undergo reductive cracking to form thiophenols, reducing the selectivity of the reaction.[36,37] To develop heterogeneous catalysts, especially single-atom catalysts with uniform active sites, it is conducive to realize high selectivity towards diaryldisulfides.

Here, single-atom Cu anchored on CeO_x nanorods is developed through the anchoring and dispersing of copper ions by terminal hydroxyl groups on the CeO_x surface. The hydroxyl-rich environment on the surface of CeO_x effectively hinders the aggregation or sintering of Cu atoms, and also realizes charge transfer through Cu–O–Ce units. The grafted single-atom Cu sites have a special valence state of between +1 and +2, and are more fully exposed to substrate molecules than embedded metal sites. Therefore, the coordination of S_2^{2-} and the oxidative addition of Ph-I can be realized at a single Cu atom, and then diphenyl disulfide can be produced efficiently through reductive elimination. Under the optimized reaction conditions, 97.1% of iodobenzene conversion and 94.8% selectivity toward diphenyl disulfide could be achieved using Cu_1/CeO_x as catalyst. Therefore, optimizing the exposure space of single-atom metal sites with flexible regulation of the electronics by the support will be conducive to multicomponent reactions to produce complex organic molecules.

Results and discussion

Synthesis and characterization of Cu_1/CeO_x nanorods

CeO_x nanorods containing defects were prepared *via* a reported method with a few modifications[38] and used as the support to fabricate the single-atom Cu catalyst (Fig. S1†). The Cu_1/CeO_x catalyst was obtained by wet impregnation using copper(II) chloride dihydrate ($CuCl_2 \cdot 2H_2O$) as the copper source and a subsequent reducing treatment. Inductively coupled plasma optical emission spectrometry (ICP-OES) revealed a Cu loading of 0.69 weight percent (wt%) in the single-atom Cu catalyst. The Cu_1/CeO_x sample was characterized by transmission electron microscopy (TEM) and scanning electron microscopy (SEM). The overall morphology was nanorods, as shown in Fig. 1a and S2,† no nanoparticles were observed in the CeO_x nanorods, and the defects of the nanorods can also be clearly observed. The energy-dispersive X-ray (EDX) elemental mapping shows that Cu and Ce are uniformly distributed on the Cu_1/CeO_x sample (Fig. 1b). Aberration corrected high-angle annular dark-field scanning transmission electron microscopy (AC HAADF-STEM) was unable to show the atomic dispersion of the Cu as the Ce atom is heavier than the Cu atom (Fig. 1c). The fast Fourier transform (FFT) results show that the included angle between each diffraction spot is 60°, which corresponds to a face-centered cubic (fcc) CeO_2 crystal (see the inset in Fig. 1c). The diffraction spot should correspond to the {220} crystal plane, which indicates that the [110] crystal plane is clearly exposed. The X-ray diffraction (XRD) pattern of Cu_1/CeO_x is the same as that of the CeO_x nanorods, without peaks attributed to copper and copper oxide

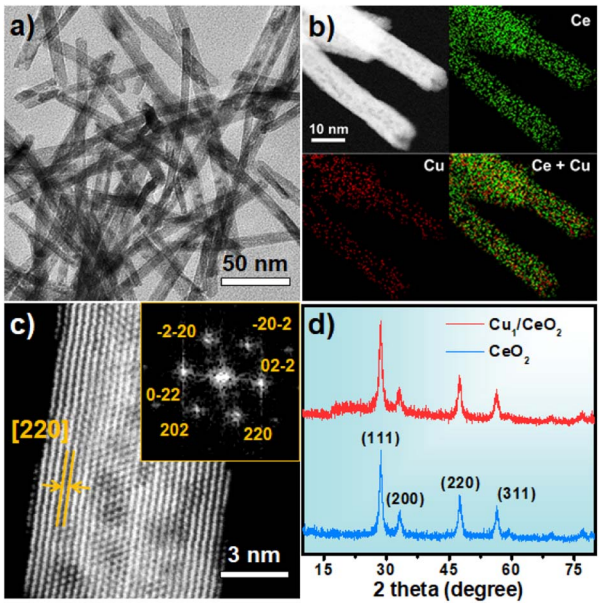

Fig. 1 (a) Representative TEM image of the Cu_1/CeO_x nanorods; (b) energy-dispersive X-ray spectroscopy for elemental mapping of the Cu_1/CeO_x nanorods; (c) representative HAADF-STEM image of a Cu_1/CeO_x nanorod; (d) XRD patterns of the Cu_1/CeO_x and CeO_x nanorods.

nanoparticles, suggesting that no changes to the crystal structure and no aggregation of Cu species occurred in the final catalysts (Fig. 1d). The Cu/CeO_x samples with higher loading (1 wt% and 2 wt%) also showed no obvious Cu nanoparticles (Fig. S3 and S4†), nor did the characteristic peaks involving Cu elements and oxides appear in the XRD data (Fig. S5†).

Compared with the X-ray absorption near edge structure spectra (XANES) of the Cu_2O and CuO standard samples, the valence state of Cu in Cu_1/CeO_x should be between +1 and +2.[39,40] Moreover, we found that the pre-edge absorption peak reflecting the 1s–4p transitions did not appear in the data of the Cu_1/CeO_x sample, while Cu_2O and CuO were located at 8982.6 eV and 8986.1 eV, respectively. This result shows that the local geometric structure of Cu in Cu_1/CeO_x is completely different from the linear O–Cu–O coordination of Cu_2O or the square coordination of oxygen atoms in CuO.[41,42] The Fourier-transform extended-edge X-ray absorption fine structure (FT EXAFS) analysis shows that the Cu K-edge spectrum of the Cu_1/CeO_x sample is different from those of Cu foil, Cu_2O and CuO, in which the Cu species are coordinated to O atoms and present atomic dispersion (Fig. 2b). The XANES absorption edge energy of the Cu/CeO_x catalyst with 1 wt% and 2 wt% loading is slightly higher than that of the Cu_1/CeO_x catalyst (Fig. S6a†), and the overall coordinative structure is still based on Cu–O bonds (Fig. S6b†). We determined the dispersion of Cu in the three catalysts through N_2O titration, among which the dispersion of the single-atom Cu was close to 100% (Table S1†). The dispersion of the Cu/CeO_x catalyst with 1 wt% and 2 wt% decreases gradually, which proves that there were unexposed Cu sites. The EXAFS fitting results show that Cu is more inclined to coordinate with two O atoms, and that the associated bond length is

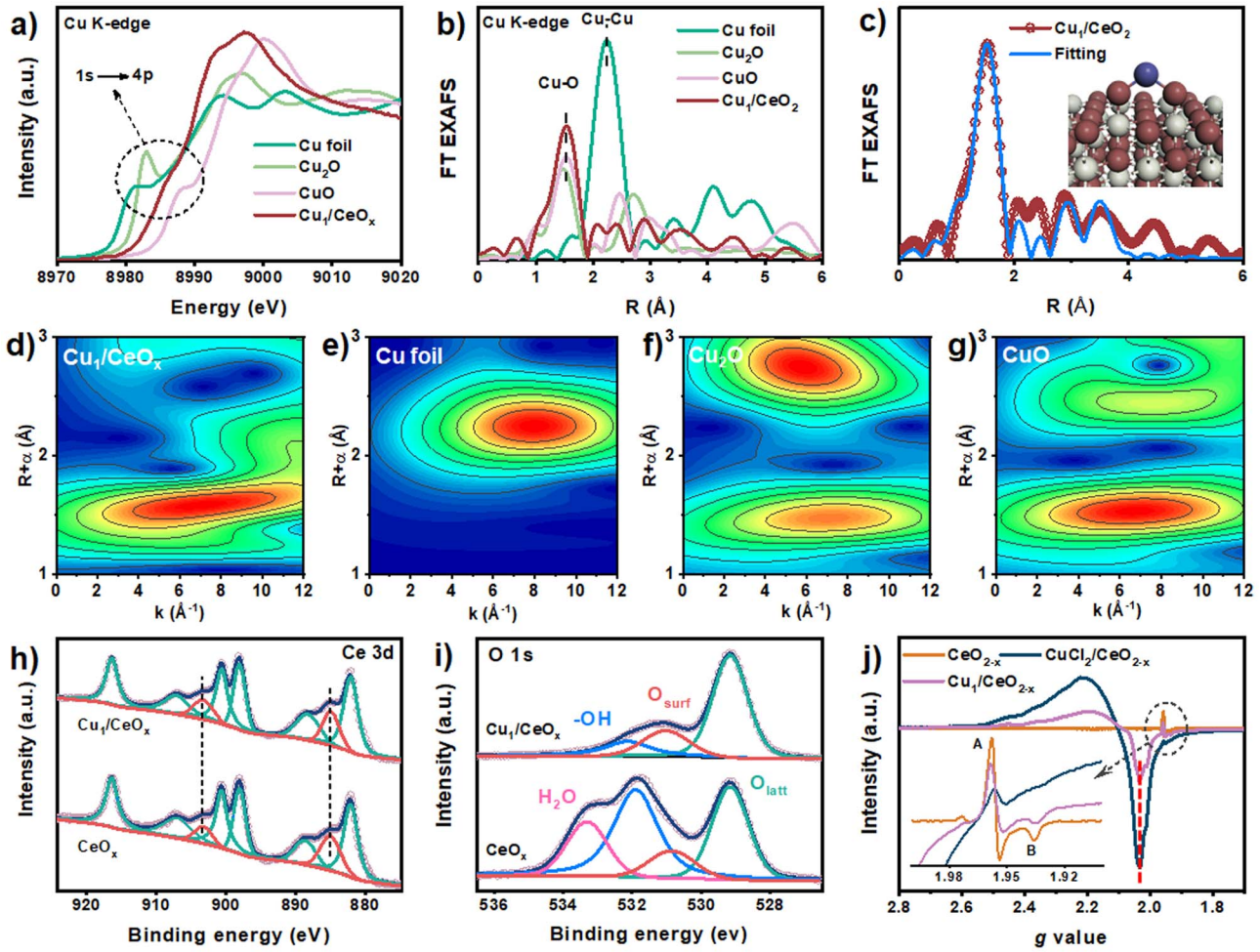

Fig. 2 (a) XANES spectra at the Cu K-edge of Cu_1/CeO_x with CuO, Cu_2O, and Cu foil; (b) FT EXAFS spectra of Cu_1/CeO_x with CuO, Cu_2O, and Cu foil; (c) the fitting curve of Cu_1/CeO_x and the experimental data, the inset shows the fitted structure; high-resolution spectra of (d) Ce 3d and (e) O 1s in the Cu_1/CeO_x and CeO_x samples; (f) EPR spectra of the CeO_x, $CuCl_2/CeO_x$ and Cu_1/CeO_x samples; (g–j) WT-EXAFS curves of the Cu_1/CeO_x, Cu_2O, CuO and Cu foil samples.

1.8 Å (Fig. 2c and S7, Table S2†). Since the length of the Ce–O bond is generally >2.3 Å, the Cu atom cannot be in any vacancy of CeO_x according to the Cu–O bond length from the EXAFS results. Therefore, the most likely structural model is single-atom Cu anchored by the oxygen atom of the hydroxyl group on the CeO_x surface, which is illustrated in the inset of Fig. 2c. We also attempted to place Cu atoms in the Ce vacancy or oxygen vacancy of CeO_x, which did not lead to ideal fitting results through comparison between the experimental Cu K-edge XANES spectra of Cu_1/CeO_x and the theoretical spectra of four different structures (Fig. S8†). The wavelet transform (WT) contour plot of Cu_1/CeO_x contains just one obvious intensity of Cu–O near 6.5 $Å^{-1}$ (Fig. 2d), while the intensity of Cu–Cu of Cu foil appears at 8.0 $Å^{-1}$ (Fig. 2e). The Cu–O coordination of the second shell in the Cu_2O and the Cu–Cu coordination of the second shell in CuO do not appear in Cu_1/CeO_x (Fig. 2f and g), which also proves the uniqueness of the Cu–O coordination structure in Cu_1/CeO_x.

X-ray photoelectron spectroscopy (XPS) data show that there is no obvious difference in the Ce 3d spectra between Cu_1/CeO_x and CeO_x, with obvious characteristic peaks of Ce^{3+} located at 885.1 eV and 903.4 eV (Fig. 2h).[43] We analyzed the O 1s spectra of CeO_x and found that CeO_x is prone to adsorbing water (H_2O, located at 533.3 eV) from the environment and formed a large number of surface hydroxyl groups (–OH, located at 532.0 eV), although the samples were all characterized after heat treatment (Fig. 2i).[44] We also obtained consistent information from the infrared spectra, in which the characteristic peak located at ~3320 cm^{-1} revealed the existence of abundant surface –OH groups on the CeO_x support (Fig. S9†). The obtained Cu_1/CeO_x sample showed an obvious signal in its XPS data for surface O species (O_{surf}, located at 530.9 eV), and the lattice O (O_{latt}, located at 529.1 eV) peak basically unchanged.[45] In the Cu 2p region, the binding energy position of Cu $2p^{3/2}$ belonging to the +1 oxidation state of Cu can be clearly observed, located at 932.5 eV (Fig. S10†).[46] There is a weak shake-up satellite peak near 940.0 eV, indicating the existence of a Cu^{2+} state.[47,48] No significant peaks were observed for Cl 2p, indicating that there is no Cl present in Cu_1/CeO_x (Fig. S11†). Through electron paramagnetic resonance (EPR) spectroscopy, as shown in Fig.

2j, the data show a Cu^{2+} signal (g value = 2.03) for the Cu_1/CeO_x nanorods, but this was less than for the unreduced $CuCl_2/CeO_x$ sample. There is no hyperfine splitting assigned to isolated Cu^{2+}, which proves the specific nature of single-atom Cu species in the Cu_1/CeO_x sample. Signals A and B can be attributed to Ce^{3+} species, which show that Ce^{3+} is the most likely oxidation state in the CeO_x support.[49] The loading of $CuCl_2$ reduces the signal intensity of Ce^{3+}, indicating that there is electron transfer from Ce^{3+} to Cu^{2+} species. This electron transfer occurs *via* a Cu–O–Ce interface, which proves the occurrence of MSI. After reduction treatment, an increase in Ce^{3+} components was observed in Cu_1/CeO_x, which is due to the electron transfer from Cu to the CeO_2 support. The Raman spectra of both CeO_x and Cu_1/CeO_x exhibit an obvious strong peak at ~457 cm^{-1}, which can be attributed to the F_{2g} fluorite structure of CeO_2 (Fig. S12†).[45] The unchanged position of this peak indicates that the introduction of Cu species does not change the overall crystal structure of the CeO_x support. The weak broad peak at ~608 cm^{-1} attributed to the defect induced (D) mode indicates that there is little difference in the oxygen vacancy concentration between the two samples.[50] The weak peak of the Cu sample at ~262 cm^{-1} can be attributed to the vibration of Cu–O bond.[51]

Catalytic performance of the Cu_1/CeO_x nanorods in the *S*-arylation reaction of iodobenzene

Iodobenzene and elemental sulfur were used as the initial exploration substrates for the *S*-arylation reaction (Fig. 3 and Table S3†). Several solvents were selected to test the catalytic performance of Cu_1/CeO_x on a dithiolation reaction at 100 °C for 12 h (Table S3†). The amount of H_2O in optimized solvent DMF had a great influence on the catalytic performance, which significantly improved the selectivity for diphenyl disulfide (**2a**). This may be due to the fact that H_2O promotes the reaction between elemental S and alkali to produce S_2^{2-}, but too much H_2O also led to a decline in catalytic activity (Table S3†). No obvious base-controlled selectivity was observed for the Cu_1/CeO_x catalyzed *S*-arylation reaction,[34] and 97.4% selectivity towards **2a** was attained with 82.6% conversion when NaOH was used as a strong base (Table S4†). When the reaction temperature was reduced, the conversion decreased significantly with a slight decrease in selectivity (Table S5,† entries 1 and 2). When the temperature rose to 110 °C, the conversion significantly increased to 97.7%, and the selectivity only slightly reduced (Table S5,† entry 4). Further increasing the reaction temperature led to a significant decrease in selectivity (Table S5,† entries 5 and 6). When the reaction time was prolonged to 14 h at 110 °C, the target product **2a** decomposed to produce phenylthiophenol (**4a**) and reduced the selectivity to 87.1% (Table S5,† entry 7). If the reaction time was shortened to 10 h, Cu_1/CeO_x achieved 97.1% conversion and 94.8% selectivity (Table S5,† entry 9). Cu/CeO_x samples synthesized with higher loading prepared and then reduced by H_2/Ar at 150 °C without washing with ultrapure water also showed poor catalytic activity (Table S5,† entries 18–21). The pure CeO_x nanorods showed no catalytic activity, where the catalyst was obtained through a synthesis method and then reduced by H_2/Ar at 150 °C. The Cu NPs showed only 34.2% transformation and 75.9% selectivity for **2a**. Therefore, CeO_x promotes the smooth *S*-arylation reaction by constructing single-atom Cu of a unique coordination environment with O atoms and charge characteristics. The Cu_1/CeO_x catalyst was stable in the *S*-arylation reaction, and the recycled catalyst retained its activity for at least four cycles (Fig. 3d, Table S6†). The ICP-OES analysis revealed a Cu loading of 0.638 wt% in the recycled Cu_1/CeO_x, which shows no difference compared to the original catalyst in the XRD patterns (Fig. S13†). Hot filtration experiments showed that almost no conversion of iodobenzene to diphenyldisulfide products was detected in the absence of the Cu catalyst, and <0.01 ppm of the Cu species was leached (Fig. S14†). These results prove that the catalysis of the *S*-arylation reaction by Cu_1/CeO_x is heterogeneous in essence, and also show that the MSI through the Cu–O–Ce interface endow the single-atom Cu with superior activity, selectivity and stability.

The Cu_1/CeO_x catalyst performed well in *S*-arylation with a wide substrate scope of aryl iodides under the optimized conditions. As summarized in Scheme 1, the *S*-arylation of iodobenzene with electron-donating groups led to higher yields being obtained. *p*-Methyl iodobenzene achieved complete conversion of iodobenzene and almost 100% selectivity of 4,4′-dimethyl-diphenyl disulfide (**2b**). The tolerance of electron-donating groups such as –Me, –OMe, –Et, –^{i}Pr and –^{t}Bu at different substitution positions enabled the synthesis of structurally diverse diaryl disulfide products (**2c**–**2i**) in moderate to good conversions and selectivity. While iodobenzene with electron-withdrawing groups underwent the *S*-arylation reaction like –F, –Cl, –Br, –CF_3 and –OCF_3 at *para*-position or *meta*-

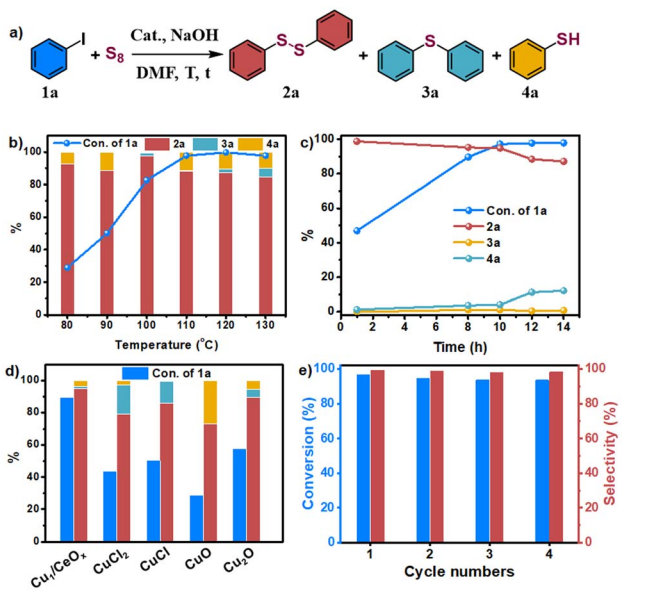

Fig. 3 (a) The reaction equation of the *S*-arylation using iodobenzene; (b) Cu_1/CeO_x catalyzed *S*-arylation using iodobenzene at different temperatures; (c) time-course plot of the conversion and different products at 110 °C; (d) catalyst comparison for the *S*-arylation reaction using iodobenzene at 110 °C for 10 h; (e) the recycling performance of Cu_1/CeO_x.

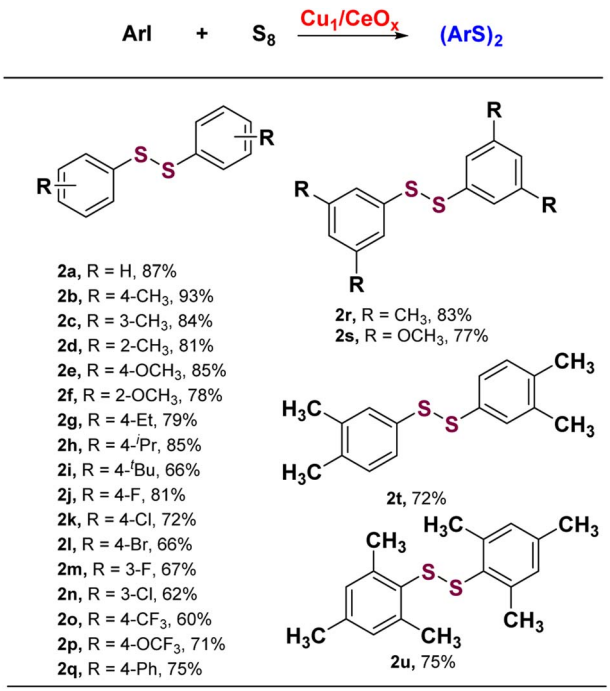

Scheme 1 Substrate scope of iodoarylene. Reaction conditions: **1** (0.5 mmol), S_8 (0.75 mmol), Cu_1/CeO_x (20 mg), NaOH (2.0 mmol), DMF (2 mL) and H_2O (67 μL), Ar, 110 °C, 10 h, isolated yield. [a]Na_2CO_3 was used as the base.

position, the yields of corresponding diaryl disulfide generally decreased slightly (**2j**–**2p**). Several aryl iodides multi-substituted at different positions underwent the *S*-arylation reaction smoothly to deliver the corresponding product in up to 86% yield (**2r**–**2t**). Even 2,4,6-trimethyliodosbenzene with steric hindrance can produce the corresponding disulfide product in 73.8% yield (**2u**). These results indicate that most of the substituted aryl iodides with various electronic and steric effects can be used to realize the *S*-arylation reaction with high efficiency and produce the corresponding diaryl disulfide products.

Control experiments and mechanism of the Cu_1/CeO_x catalyzed *S*-arylation reaction of iodobenzene

Control experiments were performed to gain insight into the mechanism of the Cu_1/CeO_x catalyzed *S*-arylation. When 2,2,6,6-tetramethyl-1-piperidinyloxy (TEMPO) or butylated hydroxytoluene (BHT) were added to the standard conditions as radical trapping reagents, almost no change in conversion and selectivity was observed, providing evidence that the Cu_1/CeO_x catalyzed *S*-arylation reaction is not a radical process (Scheme 2a and b). No products were detected when the base was removed from the standard conditions, which shows that base plays an important role in the *S*-arylation process (Scheme 2c). We also used Na_2S or Na_2S_2 to replace elemental sulfur to react under standard conditions, and almost no desired product was observed using Na_2S (Scheme 2d) but 78% conversion was observed using Na_2S_2 (Scheme 2e). NaOH reacts with elemental sulfur to form sodium thiosulfate (Na_2S_2), and the addition of

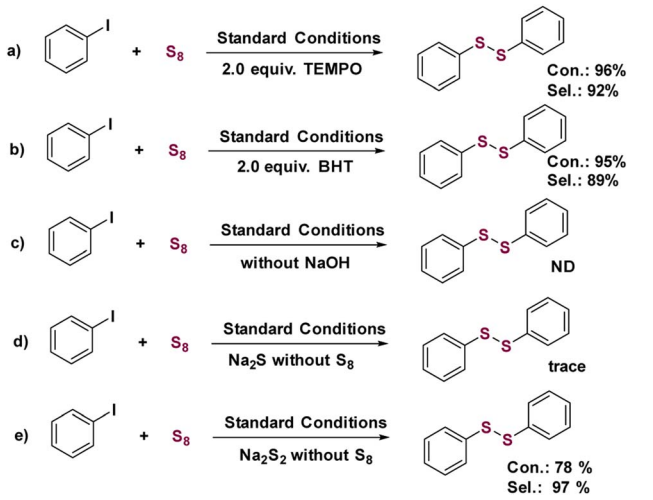

Scheme 2 Control experiments for the *S*-arylation reaction of iodobenzene with the free radical trapping reagents (a) TEMPO and (b) BHT. (c) Control experiments for the *S*-arylation reaction of iodobenzene without NaOH. (d) Control experiments for the *S*-arylation reaction of Na_2S without S_8. (e) Control experiments for the *S*-arylation reaction of Na_2S_2 without S_8.

H_2O in the solvent promotes the process. For single-atom Cu, the oxidative addition of iodobenzene must occur to form a Cu–I bond firstly before it reacts with Na_2S_2 to release NaI.

The copper halide catalysts involve the coordination of two Cu sites to S_2^{2-} firstly, and this cyclic intermediate structure is then conducive to the subsequent rupturing of S–S bonds.[34,35] The catalyst comparison results in Fig. 3d show that Cu–Cl coordination obviously produces more diphenyl sulfide than Cu–O coordination. Even if the *S*-arylation reaction is carried out without Ar protection, Cu_1/CeO_x still produces more diphenyldisulfide, while $CuCl_2$ mainly produces diphenylsulfide (Table 1). The coordination mode of single-atom Cu with S_2^{2-} is different from that of copper halide, and it is difficult to form two single-atom Cu coordinated with S_2^{2-}.

Based on the control experiment and previous studies, the mechanism of dithiolation for aryl iodides was predicted (Scheme 3). It is clear that the elemental sulfur reacts with NaOH to generate Na_2S_2,[34,35] which then reacts with the intermediate Ph–Cu^{III}–I (**I**) formed *via* the oxidative addition of Ph–I

Table 1 Comparision of Cu_1/CeO_x and $CuCl_2$ in the *S*-arylation reaction without Ar protection

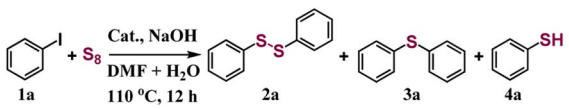

Entry	Cat	Con. (%) of **1a**	Sel. (%) **2a**	**3a**	**4a**
1	Cu_1/CeO_x	83.3	88.1	5.3	6.6
2	$CuCl_2$	61.5	38.4	59.7	1.9

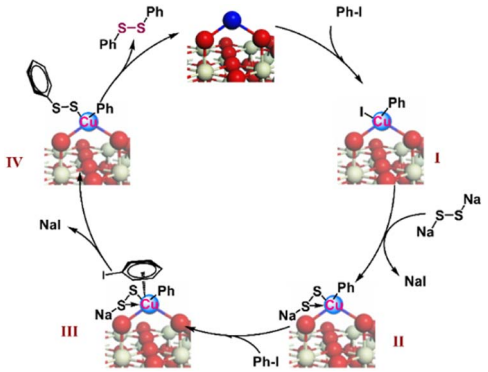

Scheme 3 The mechanism of the *S*-arylation reaction of iodobenzene with the Cu_1/CeO_x catalyst.

on single-atom Cu^I.[52,53] We speculate that the formed intermediate **II** forms a feedback bond structure, making the valence state of Cu in the intermediate **II** return to the +1 oxidation state. The Cu^I in intermediate **II** may continue to coordinate with Ph–I to provide the π-complex **III**.[54–56]

Evidence of the η^6-coordination mode of π-complex **III** can also be deduced from the substituent effect of the substrate scope, in which electro-donating substituents exhibit better reactivity than electron-withdrawing substituents. Next, intramolecular nucleophilic substitution occurs at the aromatic ring to give the intermediate **IV**, and diphenyl disulfide is finally formed *via* reductive elimination. Based on the complexity of this Ullmann-type reaction and the uncertainty of the mechanism,[57] we can only speculate its possible mechanism according to existing comparative experiments. However, the change in the oxidation state of single-atom Cu caused by the redox cycle will not result in leaching of the metal species for the MSI between CeO_x and Cu, which highlights the advantages of the single-atom Cu catalyst in the transformation of complex organic molecules. Anchoring outside the CeO_x surface fully exposes the space of single-atom Cu sites, which is conducive to the coordination and reaction of multiple substrates.

Conclusions

In summary, partially positively charged single atom Cu coordinated with two oxygen atoms was obtained *via* hydroxyl anchoring on the surface of CeO_x. This Cu_1/CeO_x catalyst realizes electron transfer through a Cu–O–Ce interface, and fully exposes the space of single-atom Cu. In the *S*-arylation reaction, the coordination and addition of multiple substrate molecules can be realized, and thus shows superior activity and specific selectivity for disulfides. Iodobenzene with substituents that exhibit different electronic properties and steric hindrance can realize the *S*-arylation reaction smoothly. Therefore, the oxide support with redox functionality is similar to organic ligands with flexible electronic regulation and more optimized spatial configuration, which makes anchored single-atom metal catalysts show promising application value in heterogeneous catalysis.

Data availability

All experimental data is available in the ESI.†

Author contributions

Yiming Zhao contributed to the investigation and formal analysis; Yan Zhou and Shanshan Lv contributed to data curation; Han Li and Qikang Wu contributed to the methodology; Shaohuan Liu, Wanying Li and Taiyu Chen contributed to resources; Zheng Chen contributed to writing the original draft.

Conflicts of interest

There are no conflicts to declare.

Acknowledgements

This work was supported by the Key Research and Development Project of Anhui Province (2022a05020048) and the Open Project of Anhui Province Key Laboratory for Degradation and Monitoring of Pollution of the Environment (FSKFKT007D). We would like to express our gratitude to Prof. Guofeng Zhao and Mr Fengyang Jiang at East China Normal University for help with the N_2O titration experiment. We thank Prof. Kun Liu at Shandong First Medical University for help with the CO adsorption.

Notes and references

1 R. Lang, X. Du, Y. Huang, X. Jiang, Q. Zhang, Y. Guo, K. Liu, B. Qiao, A. Wang and T. Zhang, *Chem. Rev.*, 2020, **120**, 11986–12043.
2 J. Park, S. Lee, H. E. Kim, A. Cho, S. Kim, Y. Ye, J. W. Han, H. Lee, J. H. Jang and J. Lee, *Angew. Chem., Int. Ed.*, 2019, **58**, 16038–16042.
3 R. Lang, T. Li, D. Matsumura, S. Miao, Y. Ren, Y.-T. Cui, Y. Tan, B. Qiao, L. Li, A. Wang, X. Wang and T. Zhang, *Angew. Chem., Int. Ed.*, 2016, **55**, 16054–16058.
4 R. Zhang, Y. Chen, M. Ding and J. Zhao, *Nano Res.*, 2022, **15**, 2810–2833.
5 Y. Wang, Z. Chen, P. Han, Y. Du, Z. Gu, X. Xu and G. Zheng, *ACS Catal.*, 2018, **8**, 7113–7119.
6 Z. Hu, C. Yang, K. Lv, X. Li, Q. Li and J. Fan, *Chem. Commun.*, 2020, **56**, 1745–1748.
7 S. Hejazi, S. Mohajernia, B. Osuagwu, G. Zoppellaro, P. Andryskova, O. Tomanec, S. Kment, R. Zbořil and P. Schmuki, *Adv. Mater.*, 2020, **32**, 1908505.
8 X. Li, H. Rong, J. Zhang, D. Wang and Y. Li, *Nano Res.*, 2020, **13**, 1842–1855.
9 S. Duan, R. Wang and J. Liu, *Nanotechnology*, 2018, **29**, 204002.
10 W. Qu, X. Liu, J. Chen, Y. Dong, X. Tang and Y. Chen, *Nat. Commun.*, 2020, **11**, 1532.
11 S. Hoang, Y. Guo, A. J. Binder, W. Tang, S. Wang, J. Liu, H. Tran, X. Lu, Y. Wang, Y. Ding, E. A. Kyriakidou, J. Yang,

T. J. Toops, T. R. Pauly, R. Ramprasad and P.-X. Gao, *Nat. Commun.*, 2020, **11**, 1062.
12 B.-H. Lee, S. Park, M. Kim, A. K. Sinha, S. C. Lee, E. Jung, W. J. Chang, K.-S. Lee, J. H. Kim, S.-P. Cho, H. Kim, K. T. Nam and T. Hyeon, *Nat. Mater.*, 2019, **18**, 620–626.
13 D. Kunwar, S. Zhou, A. DeLaRiva, E. J. Peterson, H. Xiong, X. I. Pereira-Hernández, S. C. Purdy, R. ter Veen, H. H. Brongersma, J. T. Miller, H. Hashiguchi, L. Kovarik, S. Lin, H. Guo, Y. Wang and A. K. Datye, *ACS Catal.*, 2019, **9**, 3978–3990.
14 L. F. Allard, A. Borisevich, W. Deng, R. Si, M. Flytzani-Stephanopoulos and S. H. Overbury, *J. Electron. Microsc.*, 2009, **58**, 199–212.
15 L. DeRita, J. Resasco, S. Dai, A. Boubnov, H. V. Thang, A. S. Hoffman, I. Ro, G. W. Graham, S. R. Bare, G. Pacchioni, X. Pan and P. Christopher, *Nat. Mater.*, 2019, **18**, 746–751.
16 W. Chen, H. Jin, F. He, P. Cui, C. Cao and W. Song, *Nano Res.*, 2022, **15**, 3017–3025.
17 X. Sui, L. Zhang, J. Li, K. Doyle-Davis, R. Li, Z. Wang and X. Sun, *Adv. Energy Mater.*, 2022, **12**, 2102556.
18 W. Zhang, H. Ma, H. Wang, J. Jiang, Z. Sui, Y.-A. Zhu, D. Chen and X. Zhou, *Catal. Sci. Technol.*, 2021, **11**, 7840–7843.
19 W.-H. Li, J. Yang, H. Jing, J. Zhang, Y. Wang, J. Li, J. Zhao, D. Wang and Y. Li, *J. Am. Chem. Soc.*, 2021, **143**, 15453–15461.
20 J. Yang, W.-H. Li, S. Tan, K. Xu, Y. Wang, D. Wang and Y. Li, *Angew. Chem., Int. Ed.*, 2021, **60**, 19085–19091.
21 J. Zhang, C. Zheng, M. Zhang, Y. Qiu, Q. Xu, W.-C. Cheong, W. Chen, L. Zheng, L. Gu, Z. Hu, D. Wang and Y. Li, *Nano Res.*, 2020, **13**, 3082–3087.
22 L. Chen, Z. Qi, X. Peng, J.-L. Chen, C.-W. Pao, X. Zhang, C. Dun, M. Young, D. Prendergast, J. J. Urban, J. Guo, G. A. Somorjai and J. Su, *J. Am. Chem. Soc.*, 2021, **143**, 12074–12081.
23 B. B. Sarma, J. Kim, J. Amsler, G. Agostini, C. Weidenthaler, N. Pfänder, R. Arenal, P. Concepción, P. Plessow, F. Studt and G. Prieto, *Angew. Chem., Int. Ed.*, 2020, **59**, 5806–5815.
24 S. Zhao, F. Chen, S. Duan, B. Shao, T. Li, H. Tang, Q. Lin, J. Zhang, L. Li, J. Huang, N. Bion, W. Liu, H. Sun, A.-Q. Wang, M. Haruta, B. Qiao, J. Li, J. Liu and T. Zhang, *Nat. Commun.*, 2019, **10**, 3824.
25 F. Wang, J. Ma, S. Xin, Q. Wang, J. Xu, C. Zhang, H. He and X. Cheng Zeng, *Nat. Commun.*, 2020, **11**, 529.
26 H. V. Thang, G. Pacchioni, L. DeRita and P. Christopher, *J. Catal.*, 2018, **367**, 104–114.
27 C. Liu, Y. Fang, S.-Y. Wang and S.-J. Ji, *ACS Catal.*, 2019, **9**, 8910–8915.
28 C. R. Reddy, R. Ranjan and S. K. Prajapti, *Org. Lett.*, 2019, **21**, 623–626.
29 X. S. Zhang, J. Y. Jiao, X. H. Zhang, B. L. Hu and X. G. Zhang, *J. Org. Chem.*, 2016, **81**, 5710–5716.
30 G. Liang, M. Liu, J. Chen, J. Ding, W. Gao and H. Wu, *Chin. J. Chem.*, 2012, **30**, 1611–1616.
31 G. Saito, J. A. Swanson and K.-D. Lee, *Adv. Drug Deliver. Rev.*, 2003, **55**, 199–215.
32 F. Wei, X.-Q. Shen, X.-H. Zhang and X.-G. Zhang, *Adv. Synth. Catal.*, 2018, **360**, 3911–3915.
33 R. Semwal, C. Ravi, S. Saxena and S. Adimurthy, *J. Org. Chem.*, 2019, **84**, 14151–14160.
34 H.-Y. Chen, W.-T. Peng, Y.-H. Lee, Y.-L. Chang, Y.-J. Chen, Y.-C. Lai, N.-Y. Jheng and H.-Y. Chen, *Organometallics*, 2013, **32**, 5514–5522.
35 C. Ravi, N. N. Reddy, V. Pappula, S. Samanta and S. Adimurthy, *J. Org. Chem.*, 2016, **81**, 9964–9972.
36 M. Martinek, M. Korf and J. Srogl, *Chem. Commun.*, 2010, **46**, 4387–4389.
37 Y. Li, C. Nie, H. Wang, X. Li, F. Verpoort and C. Duan, *Eur. J. Org. Chem.*, 2011, **2011**, 7331–7338.
38 Z. Chen, F.-X. Cao, W. Gao, Q.-C. Dong and Y.-Q. Qu, *Rare Met.*, 2019, **39**, 806–814.
39 D. Chen, L. H. Zhang, J. Du, H. Wang, J. Guo, J. Zhan, F. Li and F. Yu, *Angew. Chem., Int. Ed.*, 2021, **60**, 24022–24027.
40 F. Wang, J. Tian, M. Li, W. Li, L. Chen, X. Liu, J. Li, A. Muhetaer, Q. Li, Y. Wang, L. Gu, D. Ma and D. Xu, *Angew. Chem., Int. Ed.*, 2020, **59**, 8203–8209.
41 X. Hu, J. Chen, S. Li, Y. Chen, W. Qu, Z. Ma and X. Tang, *J. Phys. Chem. C*, 2020, **124**, 701–708.
42 C. Maurizio, F. d'Acapito, M. Benfatto, S. Mobilio, E. Cattaruzza and F. Gonella, *Eur. Phys. J. B*, 2000, **14**, 211–216.
43 C. Anandan and P. Bera, *Appl. Surf. Sci.*, 2013, **283**, 297–303.
44 J. Guo, X. Feng, S. Wang, Q. Wu, S. Lv, Y. Zhou, H. Li, Z. Chen and Y. Zhang, *Dalton Trans.*, 2021, **50**, 18061–18068.
45 J. Zhang, Z. Wang, W. Chen, Y. Xiong, W.-C. Cheong, L. Zheng, W. Yan, L. Gu, C. Chen, Q. Peng, P. Hu, D. Wang and Y. Li, *Chem*, 2020, **6**, 725–737.
46 Y. Xiong, S. Wang, W. Chen, J. Zhang, Q. Li, H. S. Hu, L. Zheng, W. Yan, L. Gu, D. Wang and Y. Li, *Small*, 2021, **17**, e2006834.
47 M. Yin, C.-K. Wu, Y. Lou, C. Burda, J. T. Koberstein, Y. Zhu and S. O'Brien, *J. Am. Chem. Soc.*, 2005, **127**, 9506–9511.
48 W. Wang, D. I. Sharapa, A. Chandresh, A. Nefedov, S. Heißler, L. Heinke, F. Studt, Y. Wang and C. Wöll, *Angew. Chem., Int. Ed.*, 2020, **59**, 10514–10518.
49 C. Oliva, L. Forni, A. M. Ezerets, I. E. Mukovozov and A. V. Vishniakov, *J. Chem. Soc. Faraday. Trans.*, 1998, **94**, 587–592.
50 S. Zhao, D. Kang, Y. Liu, Y. Wen, X. Xie, H. Yi and X. Tang, *ACS Catal.*, 2020, **10**, 11739–11750.
51 R. Kydd, W. Y. Teoh, K. Wong, Y. Wang, J. Scott, Q.-H. Zeng, A.-B. Yu, J. Zou and R. Amal, *Adv. Funct. Mater.*, 2009, **19**, 369–377.
52 D. Liu, H.-X. Ma, P. Fang and T.-S. Mei, *Angew. Chem., Int. Ed.*, 2019, **58**, 5033–5037.
53 Y. Jiang, Y. Qin, S. Xie, X. Zhang, J. Dong and D. Ma, *Org. Lett.*, 2009, **11**, 5250–5253.
54 D. Ma, Y. Zhang, J. Yao, S. Wu and F. Tao, *J. Am. Chem. Soc.*, 1998, **120**, 12459–12467.
55 D. Ma and Q. Cai, *Acc. Chem. Res.*, 2008, **41**, 1450–1460.
56 R. T. Stibrany, C. Zhang, T. J. Emge, H. J. Schugar, J. A. Potenza and S. Knapp, *Inorg. Chem.*, 2006, **45**, 9713–9720.
57 E. Sperotto, G. P. van Klink, G. van Koten and J. G. de Vries, *Dalton Trans.*, 2010, **39**, 10338–10351.